An Ice Breeze Mechanism for an Ice Divergence–Convergence Criterion in the Marginal Ice Zone

P. C. CHU

Department of Oceanography, Naval Postgraduate School, Monterey, CA 93943

(Manuscript received 15 December 1986, in final form 15 April 1987)

ABSTRACT

A coupled air–ice–ocean theoretical model for the marginal ice zone (MIZ) is developed and used to show that an off-ice and divergent wind field not only produces a dilation of the MIZ (as is generally thought), but also generates a compaction of MIZ for some circumstances. An ice divergence–convergence criterion in the MIZ is found and used to help explain some features, such as ice edge bands, and the formation and maintenance of polynyas and leads.

The model contains three parts: a thermally forced boundary layer air flow, a mechanically driven ice drift, and a reduced gravity ocean. The three components are linked through the surface temperature gradient and various interfacial stresses. Model results show that in the MIZ, a thermally generated surface wind blowing from ice to water (ice breeze) is generally divergent over ice owing to the maximum surface temperature gradient located at the ice edge. Such divergent local winds can make the ice flow either divergent or convergent, depending on the properties of ice and water underneath. For thin ice and a relatively deep surface water layer, the ice turning angle (angle between the direction of surface wind and ice flow) is small and the ice flow is divergent. In contrast, for thick ice and a relatively shallow surface water layer, the turning angle is large and the ice flow is convergent.

1. Introduction

In this study, a steady state coupled air–ice–ocean model is employed to investigate an ice breeze mechanism for ice divergence/convergence in the MIZ. The importance of ice breeze in the MIZ is shown as follows. Schmidt (1947) used a simple linear model to discuss seabreeze/landbreeze phenomena and concluded that for a maximum land–water temperature gradient of 4.3°C/100 km, a maximum landbreeze intensity of about 2 m s^{-1} would be reached. From observations in the Southern Bering Sea, Reynolds et al. (1985) estimated that ice floes drift to the right of the wind by approximately 30° at about 4% of the wind speed at 3 m. The ice breeze is analogous to the landbreeze. Therefore, 1°C/100 km surface temperature gradient roughly produces 0.5 m s^{-1} ice breeze, which in turn generates about 2 cm s^{-1} ice flow. The CTD data in the Central Bering Sea ice edge (Muench, 1983) show that the cross ice edge sea surface temperature (SST) gradient is around 7°C/100 km. However, the meteorological observations in the same area (Lindsay and Comiskey, 1981) indicate that the surface air temperature gradient across the ice edge is nearly 5°–10°C/100 km. Therefore, near the Bering Sea ice edge, the ice breeze is around 2.5–5 m s^{-1} (Schmidt's estimation), and the associated ice floe drift is about 10–20 cm s^{-1} (Reynold's estimation).

During September–October 1979 the Norwegian Remote Sensing Experiment was carried out in the MIZ north of Svalbard. It was found that near ice edge the wind generally blew from ice to ocean (except during 26–27 September) and the ice drift vector was deflected to the right of the wind, with a further deflection of the current in the mixed layer (Johannessen et al., 1983).

A possible mechanism for the mesoscale air–ice–ocean interaction in the MIZ is depicted in Fig. 1. The low-level air flow generated by a surface temperature gradient moves from ice to water with some deflection to the right (or left) in the north (or south) polar region. This ice breeze should have a maximum speed near the ice edge and decrease both iceward and waterward, i.e., it is divergent over the ice and convergent over the water. The ice flow driven by the surface wind field is to the right (or left) of the wind in the north (or south) polar region. The turning angle between ice flow and surface air flow varies from 0° to 90°, depending on the properties of the ice and water underneath.

The air–ice–ocean interaction model depicted in the subsequent sections is used to determine the main criterion of ice divergence/convergence.

2. Thermally forced boundary layer air flow

In this section we utilize the same planetary boundary layer model treated by Kuo (1973) and Chu (1986, 1987a,b,c,d) to simulate a thermally forced boundary layer air flow. The coordinate system is chosen such that the x-axis is in the cross ice edge direction and the

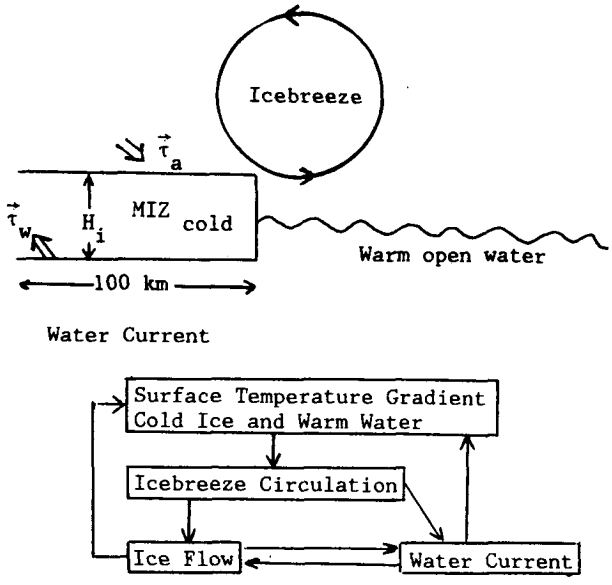

FIG. 1. Ice–air–ocean coupled system.

y-axis parallels the ice edge, as shown in Fig. 2. The x-coordinate unit length is twice the MIZ width, $L = 200$ km, and that of the vertical coordinate is $\delta = (\nu/\Omega)^{1/2}$, where ν is the vertical eddy viscosity, and Ω the angular velocity of the earth's rotation. The line $x = \frac{1}{2}$ is located at the ice edge. It is considered that spatial variations in the MIZ are much larger perpendicular to the ice edge than parallel to it, and hence derivatives with respect to y are assumed to be zero (Lepparanta and Hibler, 1985).

The potential temperature of air is divided into two parts: a basic state $\theta_{B*}(z)$ and perturbation $\theta'_*(x, z)$. The basic state is given by

$$\theta_{B*}(z) = \theta_{B0*} + (N^2\theta_{B0*}\delta/g)z, \tag{1}$$

where the subscript "$*$" means dimensional quantities, θ_{B0*} is the basic air potential temperature at the surface, and N the Brunt–Väisälä frequency. Observations show that the surface air potential temperature perturbation $\theta'_*(x, 0)$ monotonically decreases from water to ice. We use the following sinusoidal function to parameterize the surface thermal condition:

$$\theta'_*(x, 0) = -\mathrm{D}T_0 \cos\pi x_*/L, \tag{2}$$

where $\mathrm{D}T_0$ is the characteristic temperature difference across the MIZ. The coordinates and atmospheric variables are nondimensionalized by setting

$$\left.\begin{aligned} (x_*, z_*) &= (xL, z\delta) \\ s' = \theta'_*/\theta_{B0} &= (\mathrm{D}T_0/\theta_{B0})s^{(a)} \\ (u_*^{(a)}, v_*^{(a)}, w_*^{(a)}) &= U(u^{(a)}, v^{(a)}, w^{(a)}\delta/L) \\ P_*^{(a)} &= (g\delta\mathrm{D}T_0/\theta_{B0})p^{(a)} \\ \delta &= (\nu/\Omega)^{1/2}, \end{aligned}\right\} \tag{3}$$

where

$$U \equiv g\delta\mathrm{D}T_0/(2L\Omega\theta_{B0}) \tag{4}$$

is the scale of icebreeze wind. If we assume that the local air flow satisfies the modified Boussinesq approximation (Kuo, 1973), the vorticity equation, the momentum equation (both in y direction), and the heat equation for the air disturbances generated by differential surface temperature gradient near the MIZ are (Chu, 1986, 1987a,b,c,d)

$$E\partial^4\Psi^{(a)}/\partial z^4 = f_0\partial v^{(a)}/\partial z - \partial s^{(a)}/\partial x, \tag{5}$$

$$E\partial^2 v^{(a)}/\partial z^2 = -f_0\partial\Psi^{(a)}/\partial z, \tag{6}$$

$$E\partial^2 s^{(a)}/\partial z^2 = \mathrm{Ri}\partial\Psi^{(a)}/\partial x. \tag{7}$$

In the foregoing,

$$u^{(a)} = -\partial\Psi^{(a)}/\partial z, \quad w^{(a)} = \partial\Psi^{(a)}/\partial x, \tag{8}$$

where $f_0 = \sin\varphi$, φ is the latitude, and

$$\left.\begin{aligned} E &\equiv \nu/(2\Omega\delta^2) = \tfrac{1}{2} \\ \mathrm{Ri} &\equiv (\delta N/2L\Omega)^2 \end{aligned}\right\} \tag{9}$$

are the Ekman and Richardson numbers, respectively. Eliminating $v^{(a)}$ and $s^{(a)}$ from (5)–(7) we find that the streamfunction satisfies the following partial differential equation:

$$\left(\frac{1}{4}\partial^4/\partial z^4 + f_0^2\right)\partial^2\Psi^{(a)}/\partial z^2 + \mathrm{Ri}\partial^2\Psi^{(a)}/\partial x^2 = 0. \tag{10}$$

We solve (10) for the streamfunction $\Psi^{(a)}$, and obtain the solutions of $v^{(a)}$ and $s^{(a)}$ from (6) and (7) after substituting $\Psi^{(a)}$. The local air flow is thermally forced by the surface temperature gradient as indicated in (2), therefore the streamfunction should be written as

$$\Psi^{(a)}(x, z) = \Psi^{(a)}(z)\sin\pi x. \tag{11}$$

The boundary conditions in the vertical direction are derived as follows. The dependent variables should remain finite as $z \to \infty$, i.e.,

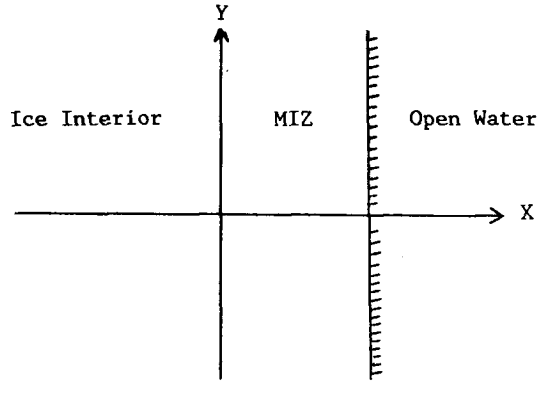

FIG. 2. The model MIZ and the coordinate system.

$$\lim_{z\to\infty}(|\Psi^{(a)}|, |\partial\Psi^{(a)}/\partial z|, |v^{(a)}|, |s^{(a)}|) < \infty. \quad (12)$$

The boundary conditions at $z = 0$ are

$$\Psi^{(a)} = 0, \quad \partial\Psi^{(a)/\partial z} = M\partial^2\Psi^{(a)}/\partial z^2,$$
$$v^{(a)} = M\partial v^{(a)}/\partial z, \quad s^{(a)} = -\cos\pi x, \quad (13)$$

where M is a measure of the effective depth of the constant stress-sublayer (Kuo, 1973). Substituting (11) into (10) we obtain the following sixth order ordinary differential equation for the Fourier coefficient $\Psi^{(a)}$:

$$d^6\Psi^{(a)}/dz^6 + 4f_0^2 d^2\Psi^{(a)}/dz^2 - 4\pi^2\,\mathrm{Ri}\Psi^{(a)} = 0. \quad (14)$$

The general solution of (14) has the following form:

$$\Psi^{(a)}(z) = \sum_{j=1}^{6} a_j \exp(\lambda_j z), \quad (15)$$

where the eigenvalues λ_j ($j = 1, 2, \cdots, 6$) are the roots of the sixth-order algebraic equation:

$$\lambda^6 + 4f_0^2\lambda^2 - 4\pi^2\,\mathrm{Ri} = 0. \quad (16)$$

According to the upper boundary conditions listed in (12) we must set up coefficients which correspond to those eigenvalues with positive real parts equal to zero. Consequently the general solution (16) satisfying the top boundary conditions may be written:

$$\Psi^{(a)}(z) = \sum_{j=1}^{3} a_j \exp(\lambda_j z), \quad (17)$$

where the eigenvalues λ_j all have negative real parts. Substituting (17) into (11) we obtain the streamfunction

$$\Psi^{(a)}(x, z, t) = \sum_{j=1}^{3} a_j \exp(\lambda_j z)\sin\pi x. \quad (18)$$

Integrating the momentum equation (6) and the heat equation (7) with respect to z after substituting (18), we find that $v^{(a)}$ and $s^{(a)}$ are given by

$$v^{(a)}(x, z) = b - 2f_0\sum_{j=1}^{3}(a_j/\lambda_j)\exp(\lambda_j z)\sin\pi x, \quad (19)$$

$$s^{(a)}(x, z) = 2\pi\,\mathrm{Ri}\sum_{j=1}^{3}(a_j/\lambda_j^2)\exp(\lambda_j z)\cos\pi x. \quad (20)$$

Substituting the solutions (18)–(20) into the surface boundary conditions listed in (13) we obtain the following four algebraic equations for a_j and b:

$$\sum_{j=1}^{3} a_j = 0, \quad (21)$$

$$\sum_{j=1}^{3}\lambda_j(1 - M\lambda_j)a_j = 0, \quad (22)$$

$$-2f_0\sum_{j=1}^{3}(a_j/\lambda_j)(1 - M\lambda_j) + b = 0, \quad (23)$$

$$2\pi\,\mathrm{Ri}\sum_{j=1}^{3} a_j/\lambda_j^2 = -1. \quad (24)$$

The four constants a_1, a_2, a_3 and b can be readily obtained by solving the four linear nonhomogeneous algebraic equations.

The surface wind (dimensional form) driven by the horizontal temperature gradient is computed by

$$u_*^{(a)}(x, 0) = u_{0*}{}^{(a)}\sin\pi x, \quad (25)$$

$$v_*^{(a)}(x, 0) = v_{0*}{}^{(a)}\sin\pi x, \quad (26)$$

where

$$u_{0*}{}^{(a)} \equiv U\,\mathrm{Re}(\sum_{j=1}^{3} a_j\lambda_j) \quad (27)$$

$$v_{0*}{}^{(a)} \equiv U\,\mathrm{Re}[b - 2f_0\sum_{j=1}^{3}(a_j/\lambda_j)]. \quad (28)$$

The purpose of using the nondimensional form for the atmosphere is to get solutions that simply show the magnitude of the boundary layer air flow. After obtaining solutions (27) and (28), we will use dimensional variables. The subscript "*" will be dropped. Figure 3 shows the cross-ice-edge atmospheric circulation $(u^{(a)}, w^{(a)})$ at $\varphi = 75°\mathrm{N}$, $DT_0 = 6$ K (mean temperature gradient $\pi DT_0/L = 9.4°\mathrm{C}/100$ km) and $N = 10^{-2}\ \mathrm{s}^{-1}$. We see the obvious ice breeze at low levels. The speed of the ice breeze reaches a maximum (which is around 4 m s^{-1}) at the ice edge, which is consistent with Schmidt's (1947) results.

3. Free ice drift model

Roed and O'Brien (1983) show that the internal ice stress and the nonlinear terms are not crucial for the MIZ dynamics, and that the ice velocity is an order of magnitude larger than water current in the MIZ. Following their theoretical model, the momentum equations for a free drift ice model are

$$fv^{(i)} + [\tau_x{}^{(a,i)} + \tau_x{}^{(w,i)}]/(\rho_i H_i) = 0, \quad (29)$$

$$-fu^{(i)} + [\tau_y{}^{(a,i)} + \tau_y{}^{(w,i)}]/(\rho_i H_i) = 0, \quad (30)$$

where f ($= 2\Omega\sin\varphi$) is the Coriolis parameter, $\mathbf{V}^{(i)} = (u^{(i)}, v^{(i)})$ the ice velocity, H_i the mean ice thickness, ρ_i the ice density, $\vec{\tau}^{(a,i)} = (\tau_x{}^{(a,i)}, \tau_y{}^{(a,i)})$ the wind stress on ice, $\vec{\tau}^{(w,i)} = (\tau_x{}^{(w,i)}, \tau_y{}^{(w,i)})$ the water stress on ice. The air and water stresses on ice are computed by

$$\vec{\tau}^{(a,i)} = \rho_a C_{ai}\mathbf{V}^{(a)} \quad (31)$$

$$\vec{\tau}^{(w,i)} = \rho_w C_{wi}[\mathbf{V}^{(w)} - \mathbf{V}^{(i)}], \quad (32)$$

where C_{ai} and C_{wi} are dimensional (m s^{-1}) air and water drag coefficients (on ice); ρ_a and ρ_w are the densities of air and surface water, respectively; $\mathbf{V}^{(a)} = (u^{(a)}, v^{(a)})$ is the surface wind, and $\mathbf{V}^{(w)} = (u^{(w)}, v^{(w)})$ the water velocity.

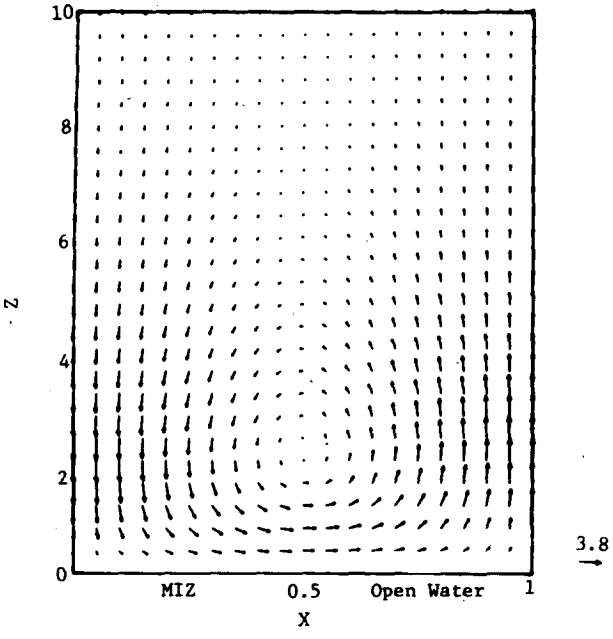

FIG. 3. Thermally forced ice breeze circulation in the cross-ice section with u in m s^{-1} and w in cm s^{-1}.

4. Reduced gravity ocean model

Suppose that the ocean is composed of two layers, in which the horizontal inhomogeneity of density inside the same layer is much smaller than the density difference between the two layers, and the lower layer is deep enough for motion in the lower layer to be vanishingly small. Such a model is referred to as a reduced-gravity model. Furthermore, the model has the simplest form of dissipation, namely, Rayleigh friction with decay rate R and Newtonian cooling, also with decay rate R. The momentum and continuity equations for the ocean are written by (Gill, 1982; Roed and O'Brien, 1983)

$$Ru^{(w)} - fv^{(w)} = -g^*\partial h^{(w)}/\partial x + [(1-A)\tau_x^{(a,w)} + A\tau_x^{(i,w)}]/(\rho_w H_w) \quad (33a)$$

$$Rv^{(w)} + fu^{(w)} = [(1-A)\tau_y^{(a,w)} + A\tau_y^{(i,w)}]/(\rho_w H_w) \quad (33b)$$

$$Rh^{(w)} + H_w \partial u^{(w)}/\partial x = 0, \quad (33c)$$

where g^* is a reduced gravitational acceleration, H_w the equilibrium depth of the pycnocline, $h^{(w)}$ the thickness of the upper layer, and $\vec{\tau}^{(i,w)} = (\tau_x^{(i,w)}, \tau_y^{(i,w)})$ the ice stress on the water. $\vec{\tau}^{(i,w)}$ has the same magnitude but the opposite direction as $\vec{\tau}^{(w,i)}$, i.e.,

$$\vec{\tau}^{(i,w)} = -\vec{\tau}^{(w,i)} = -\rho_w C_{wi}(\mathbf{V}^{(w)} - \mathbf{V}^{(i)}). \quad (33d)$$

Here A is the ice compactness or ice concentration (i.e., the fraction of area covered by ice). Hibler and Ackley (1983) took the 50% limit of A as the ice edge. Inside the MIZ, the ice concentration, A, decreases waterward very slowly from the boundary between pack ice and the MIZ (where $A \sim 1$) to some place near the ice edge, and then diminishes very rapidly to the ice edge. If the area we focus on is not very close to the ice edge, we may set $A \sim 1$. The portion of air stress on the water, $(1-A)\vec{\tau}^{(a,w)}$, is then neglected compared to the ice stress on the water, $A\vec{\tau}^{(i,w)}$. Setting $A = 1$ and eliminating $h^{(w)}$ from (33a) and (33c), the momentum equations (33a) and (33b) become

$$Ru^{(w)} - fv^{(w)} - (g^*H_w/RL^2)\partial^2 u^{(w)}/\partial x^2 = \tau_x^{(i,w)}/(\rho_w H_w) \quad (34)$$

$$Rv^{(w)} + fu^{(w)} = \tau_y^{(i,w)}/(\rho_w H_w). \quad (35)$$

TABLE 1. The standard model parameters.

$L = 200$ km	$\nu = 5\ \mathrm{m^2 s^{-1}}$	$\nu_h = 10^5\ \mathrm{m^2 s^{-1}}$
$\Omega = 0.7292 \times 10^{-4}\ \mathrm{s^{-1}}$	$g = 9.81\ \mathrm{m s^{-2}}$	$R = 2.08 \times 10^{-5}\ \mathrm{s^{-1}}$
$\theta_{B0^*} = 270$ K	$C_{wi} = 0.86 \times 10^{-3}\ \mathrm{m s^{-1}}$	$C_{ai} = 0.03\ \mathrm{m s^{-1}}$
$\rho_a = 1.29\ \mathrm{kg m^{-3}}$	$\rho_w = 1000\ \mathrm{kg m^{-3}}$	$\rho_i = 910\ \mathrm{kg m^{-3}}$
$g^* = 0.005\ \mathrm{m s^{-2}}$	$DT_0 = 6$ K	

5. Ice divergence–convergence criterion

The surface wind is the forcing term of the ice–ocean system. Since our model is linear, the mechanically forced ice and water motion $\mathbf{V}^{(i)}$ and $\mathbf{V}^{(w)}$ should have the same Fourier component as the forcing term $\mathbf{V}^{(a)}$, i.e.,

$$u^{(i)} = u_0^{(i)} \sin\pi x, \quad v^{(i)} = v_0^{(i)} \sin\pi x, \quad (36)$$

$$u^{(w)} = u_0^{(w)} \sin\pi x, \quad v^{(w)} = v_0^{(w)} \sin\pi x. \quad (37)$$

Substituting (31), (32), (33d), (36) and (37) into (29), (30), (34) and (35) we have the following four linear algebraic equations for the Fourier coefficients $u_0^{(w)}$, $v_0^{(w)}$, $u_0^{(i)}$ and $v_0^{(i)}$:

$$[R + \pi^2 g^*/(RL^2) + \omega_3]u_0^{(w)} - fv_0^{(w)} - \omega_3 u_0^{(i)} = 0, \quad (38)$$

$$fu_0^{(w)} + (R + \omega_3)v_0^{(w)} - \omega_3 v_0^{(i)} = 0, \quad (39)$$

$$-\omega_2 u_0^{(w)} + \omega_2 u_0^{(i)} - fv_0^{(i)} = \omega_1 u_0^{(a)} \quad (40)$$

$$-\omega_2 v_0^{(w)} + \omega_2 v_0^{(i)} + fu_0^{(i)} = \omega_1 v_0^{(a)}, \quad (41)$$

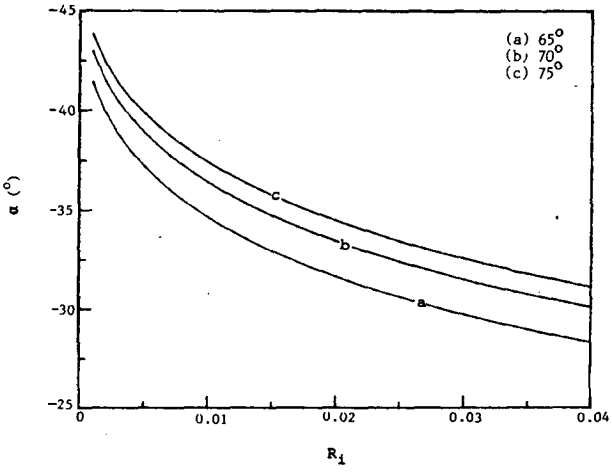

FIG. 4. Dependence of α on the atmospheric Richardson number Ri for three different latitudes: (a) 65°, (b) 70° and (c) 75°.

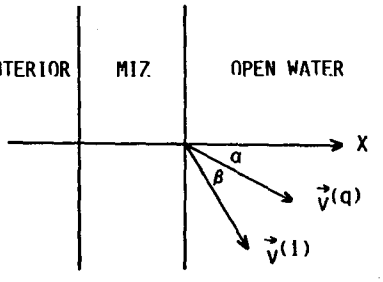

FIG. 5. Air deflection angle α and ice turning angle β.

where parameters ω_1, ω_2 and ω_3 are defined by

$$\omega_1 = \rho_a C_a/(\rho_i H_i), \quad \omega_2 = \rho_w C_w/(\rho_i H_i), \quad \omega_3 = C_w/H_w. \tag{42}$$

Solving the nonhomogeneous linear algebraic equations (38)–(41) we obtain

$$u_0^{(i)} = \omega_1[\omega_2(1-\alpha_2)u_0^{(a)} + f(1+\alpha_3\omega_2)v_0^{(a)}]/ [\omega_2^2(1-\alpha_1)(1-\alpha_2) + f(1+\alpha_3\omega_2)^2], \tag{43}$$

$$v_0^{(i)} = \omega_1[\omega_2(1-\alpha_1)v_0^{(a)} - f(1+\alpha_3\omega_2)u_0^{(a)}]/ [\omega_2^2(1-\alpha_1)(1-\alpha_2) + f(1+\alpha_3\omega_2)^2], \tag{44}$$

$$u_0^{(w)} = \omega_3[u_0^{(i)}(R+\omega_3) + f v_0^{(i)}]/[\alpha_0(R+\omega_3) + f^2] \tag{45}$$

$$v_0^{(w)} = \omega_3[\alpha_0 v_0^{(i)} - f u_0^{(i)}]/[\alpha_0(R+\omega_3) + f^2] \tag{46}$$

where

$$\alpha_0 \equiv R + \omega_3 + \pi^2 g^* H_w/(RL^2)$$

$$\alpha_1 \equiv \omega_3(R+\omega_3)/[\alpha_0(R+\omega_3) + f^2]$$

$$\alpha_2 \equiv \omega_3\alpha_0/[\alpha_0(R+\omega_3) + f^2]$$

$$\alpha_3 \equiv \omega_3/[\alpha_0(R+\omega_3) + f^2]. \tag{47}$$

Table 1 lists the parameter values for the present calculations. Figure 4 describes the dependence of the ice breeze deflection angle (angle between surface temperature gradient and surface wind) $\alpha = \tan^{-1}(v_0^{(a)}/u_0^{(a)})$ on Ri at three different latitudes (65°, 70° and 75°). The $|\alpha|$ increases with increasing latitude and decreases with increasing Ri. At 65° (N and S) latitude it varies from 41.8° when Ri = 10^{-3} to $\alpha = 27.5°$ when Ri = 4×10^{-2}.

The angle between surface wind and ice velocity, β (as shown in Fig. 5), is defined by

$$\beta = \tan^{-1}(v_0^{(i)}/u_0^{(i)}) - \alpha \tag{48}$$

where $u_0^{(i)}$ and $v_0^{(i)}$ are computed by (43) and (44). An ice divergence–convergence criterion is simply

$$|\alpha+\beta| \begin{cases} > \pi/2, & \text{ice convergence} \\ < \pi/2, & \text{ice divergence.} \end{cases} \tag{49}$$

We compute the ice turning angle β as a function of H_i and H_w for $\varphi = 65°$, where H_i varies from 0 to 10 m and H_w from 0 to 50 m. The distribution of β with H_i and H_w is shown in Fig. 6. Small values of $|\beta|$ (small turning angles) are located in the region of large H_w and small H_i. The smaller the H_i (or the larger the H_w), the smaller the $|\beta|$. It is quite understandable that the water current $\mathbf{V}^{(w)}$ is very weak as H_w becomes large, due to small mechanical forcing terms $\omega_3 u^{(i)}$ and $\omega_3 v^{(i)}$ in (38) and (39). When the water current is weak (due to large H_w) the turning angle largely depends on the ice thickness. For thin ice, $w_1 \gg f$, (40) and (41) show that $\mathbf{V}^{(i)}$ deflects by small angle from $\mathbf{V}^{(a)}$, therefore the ice flow is divergent.

Solving the algebraic equation (48) for H_i after setting $|\alpha + \beta| = \pi/2$, we get the dependence of H_i on H_w for

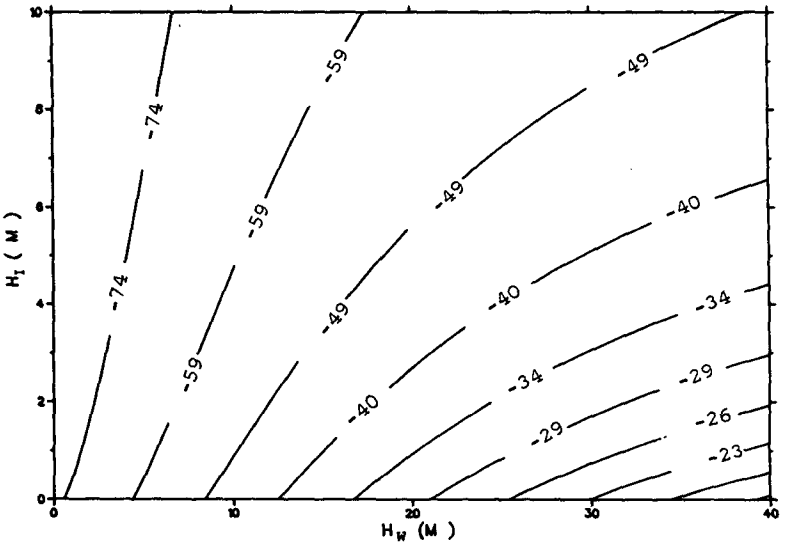

FIG. 6. Isolines of β (°) in the (H_i, H_w) plane for $\varphi = 65°$.

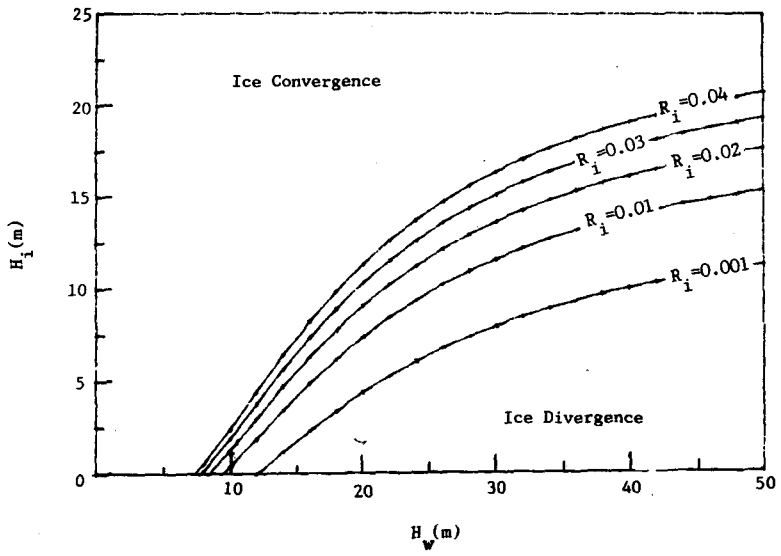

FIG. 7. H_i–H_w curves for zero ice divergence–convergence for five different values of Ri.

the no convergence or divergence case, as shown in Fig. 7. The curves separate the parameter plane (H_i, H_w) into ice convergence and ice divergence parts. We can differentiate between ice divergence and ice convergence due to the ice breeze in the MIZ by the parameters Ri, H_i, and H_w. If the drag coefficient C_{wi} is doubled, the turning angle β only has minor changes (less than 10%).

6. Conclusion

(i) This air–ice–ocean model is intended to depict only the mesoscale processes of air–ice–ocean interaction in the MIZ. The synoptic-scale pressure gradient may additionally produce surface winds, and in turn drive ice drift. These processes are, however, beyond the scope of this paper. Nevertheless, when the ice-to-open-water temperature gradient is strong, the ice breeze mechanism discussed here may become as strong as, or stronger than, the synoptic forcing.

(ii) The model shows the different effects of ice breeze on ice flow, and gives an ice divergence–convergence criterion in the MIZ, which may help to understand the formation of ice edge bands, and the formation and maintenance of polynyas and leads.

(iii) It should be stressed, however, that the model cannot be used to describe the system with an oceanic density front paralleling the ice edge as observed by Muench and Schumacher (1985).

Acknowledgments. The author is grateful to Prof. H. L. Kuo of the University of Chicago and Prof. R. W. Garwood of the Naval Postgraduate School for invaluable discussion and comments. The reviewers' comments are also highly appreciated.

This research was supported by Grant ATM 83-14206 from the National Science Foundation.

REFERENCES

Chu, P. C., 1986: An instability theory of ice–air interaction for the migration of the marginal ice zone. *Geophys. J. R. Astronom. Soc.*, **86**, 863–883.

——, 1987a: An instability theory of ice–air interaction for the formation of ice edge bands. *J. Geophys. Res.*, **92**, 6966–6970.

——, 1987b: Generation of unstable modes of the iceward attenuating swell by icebreeze. *J. Phys. Oceanogr.*, **17**, 828–832.

——, 1987c: An air–sea feedback mechanism for quasi-geostrophic water movement near a fast shelf-ice edge with a small curvature. *Chinese J. Atmos. Sci.*, in press.

——, 1987d: A seabreeze mechanism for ice edge upwelling. *Chinese J. Atmos. Sci.*, in press.

Gill, A. E., 1982: *Atmosphere–Ocean Dynamics.* Academic Press, 466 pp.

Hibler, W. D. III, and S. F. Ackley, 1983: Numerical simulation of the Weddell Sea pack ice. *J. Geophys. Res.*, **88**, 2873–2887.

Johannessen, O. M., J. A. Johannessen, J. Morison, B. A. Farrelly and E. A. S. Svendsen, 1983: Oceanographic conditions in the marginal ice zone north of Svalbard in early fall 1979 with an emphasis on mesoscale processes. *J. Geophys. Res.*, **88**, 2755–2769.

Kuo, H. L., 1973: Planetary boundary layer flow of a stable atmosphere over the globe. *J. Atmos. Sci.*, **30**, 53–65.

Lepparanta, M., and W. D. Hibler, 1985: On the role of plastic ice interaction in marginal ice zone dynamics. *J. Geophys. Res.*, **90**, 11 899–11 909.

Lindsay, R. W., and A. L. Comiskey, 1981: Surface and upper-air observations in the eastern Bering Sea, February and March. NOAA Tech. Memo. ERL-PMEL-35, 90 pp., Washington, DC.

Muench, R. D., 1983: Mesoscale oceanographic features associated with the central Bering Sea ice edge: February–March 1981. *J. Geophys. Res.*, **88**, 2715–2722.

——, and J. D. Schumacher, 1985: On the Bering Sea ice edge front. *J. Geophys. Res.*, **90**, 3185–3197.

Reynolds, M., C. H. Pease and J. E. Overland, 1985: Ice drift and regional meteorology in the southern Bering Sea: Results from MIZEX West. *J. Geophys. Res.*, **90**, 11 967–11 981.

Roed, L. P., and J. J. O'Brien, 1983: A coupled ice–ocean model of upwelling in the marginal ice zone. *J. Geophys. Res.*, **88**, 2863–2872.

Schmidt, F. H., 1947: An elementary theory of the land- and sea-breeze circulation. *J. Meteor.*, **4**, 9–15.